Supplementary Material (ESI) for Journal of Materials Chemistry

Impact of Contact Evolution on the Shelf Life of Organic Solar Cells

By *Matthew T. Lloyd*, *Dana C. Olson*, *Ping Lu*, *Erica Fang*, *Diana L. Moore, Matthew S. White, Matthew O. Reese, David S. Ginley*, and *Julia W. P. Hsu*

Supporting Information

Solar Cell Performance Parameters

Figure S1 displays the normalized short-circuit current (J_{sc}), fill factor (FF), and open-circuit voltage (V_{oc}) for each device geometry for the duration of the shelf-life study. In order to compare the relative changes in these parameters between devices, each parameter is normalized by the value measured immediately after device fabrication. Rapid decay is apparent for all three parameters for devices utilizing Ag negative electrodes, with and without the PEDOT:PSS layer. For the ITO/BHJ/Ag device (black curve), we omit data points after day 10 when the device polarity inverts. The relatively small change in FF for this device originates from the low initial value of the FF (27%). Devices with Ca/Al electrodes display relatively stable V_{oc} over time, while the J_{sc} shows an exponential decay after the second testing session. The device parameters for the ITO/ZnO/BHJ/Ag device increase up to ~10 days, after which the J_{sc} also follows a fast decay. The ITO/ZnO/P3HT/Ag device shows relatively stable parameters, with J_{sc} increasing by 21% after day 40.

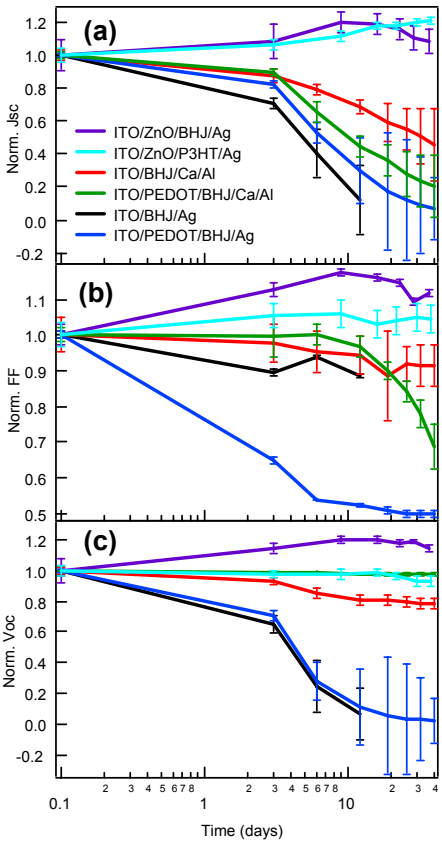

Fig. S1. Normalized (a) short-circuit current (J_{sc}), (b) fill factor (FF), and (c) open-circuit voltage (V_{oc}) measured over the course of 40 days.

EELS Mapping

Electron energy-loss spectroscopy (EELS) was used to map the distribution of Ca and oxygen in ITO/BHJ/Ca/Al devices after aging. **Figure S2a** shows the bright field TEM image of the device cross-section, and **Fig. S2b** and **S2c** show the Ca and oxygen map for the same field of view, respectively. The location of the porous layer is evident in each micrograph (bright white in Fig. S2a and dark in Fig. S2b and S2c) and can be used as a point of reference to compare micrographs. The Ca map in Fig. S2b illustrates that the strongest signal for elemental Ca originates on the BHJ side of the porous layer. On the Al side of the porous layer, the Ca signal appears comparatively less intense. In Fig. S2c, the elemental oxygen signal is equally intense on either side of the porous layer. Due to the significant overlap of the Ca and oxygen signals, we are led to believe that the Ca layer is oxidized, and the enhanced oxygen signal on the Al side of the void layer indicates that Al is forming an oxide layer at the Ca-Al interface as well. Overall, these maps are in good agreement with the Auger profiles (**Fig. S3** and Fig. 2c of the manuscript).

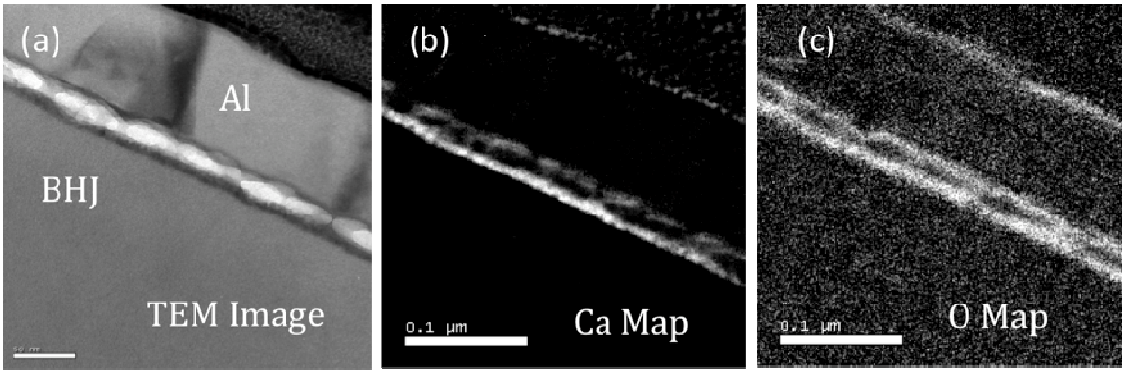

Fig. S2 (a) Bright field TEM image of an ITO/BHJ/Ca/Al device after aging. EELS map of elemental (b) Ca and (c) oxygen.

Auger Depth Profile

Auger depth profiles were recorded for the ITO/BHJ/Ca/Al sample as freshly prepared (shown in **Fig. S3**) and after aging (shown in Fig. 2c of the manuscript). To minimize exposure to oxygen and moisture, the freshly prepared samples were removed from the vacuum chamber in a nitrogen glove box, transferred to a hermetically sealed stainless steal transport vessel, and exposed to air briefly during loading into the Auger microscope. Comparing Fig. 2c and Fig. S3, it is apparent that the depth profiles of the fresh and aged samples are remarkably similar. The most surprising observation lies in the fact that the freshly prepared sample has an equally prominent oxygen peak at the Ca-Al interface. This indicates that oxide formation occurs either during the metallization process or immediately thereafter. As discussed in the manuscript, this supports the notion that physical degradation (i.e. loss in contact area) between the BHJ and the Ca/Al electrode is primarily responsible for the increase in series resistance and the degradation in photocurrent. Also evident in Fig. S3 is an increase in the oxygen signal throughout the thickness of the Al electrode, which was observed for more than one depth profile on the same sample. A similar oxygen signal within the bulk of the Al electrode was not observed for the sample shown in Fig. 2c of the manuscript, which was aged at ambient atmosphere for >40 days. For the sample in Fig. S3, we speculate that a partial pressure of oxygen during Al deposition of this device oxidized the full thickness Al film.

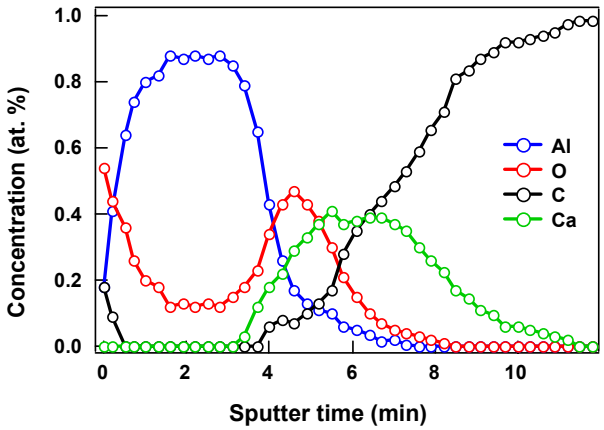

Fig. S3 Elemental Analysis depth profile as determined by Auger spectroscopy for a freshly prepared ITO/BHJ/Ca/Al device.

I-V and EQE Behavior for ITO/BHJ/Ag Devices

Figure S4a shows the *I-V* behavior for an ITO/BHJ/Ag device, the normalized parameters for which are shown in Fig. S1 and Fig. 1 (black curve) of the manuscript. These curves are interesting in that they show the incremental change in device polarity. Initially the work function of Ag is lower than that of ITO, and the built-in field drives electrons toward the Ag electrode. Eventually (after *Test 3*) the work function of Ag increase beyond that of ITO and a switch in polarity drives electrons to be extracted by the ITO. The initial test (black curve) shows rectification (albeit of a low value) where forward bias is marked by positive current flow under positive applied bias. The final test (red curve) shows slight rectification with forward bias now defined by negative current flow under negative applied bias. Series resistance, calculated as the inverse slope near -1 V or +1 V, tends to decrease with each successive test.

Figure S4b shows the EQE for an ITO/BHJ/Ag device measured immediately after fabrication and after aging for 40 days. Initially, electrons are collected by the Ag, and after aging, electrons are collected by the ITO. Hence, the polarity for the aged EQE measurement is reversed. Despite the change in polarity, the shape of the normalized EQE does not change significantly upon aging.

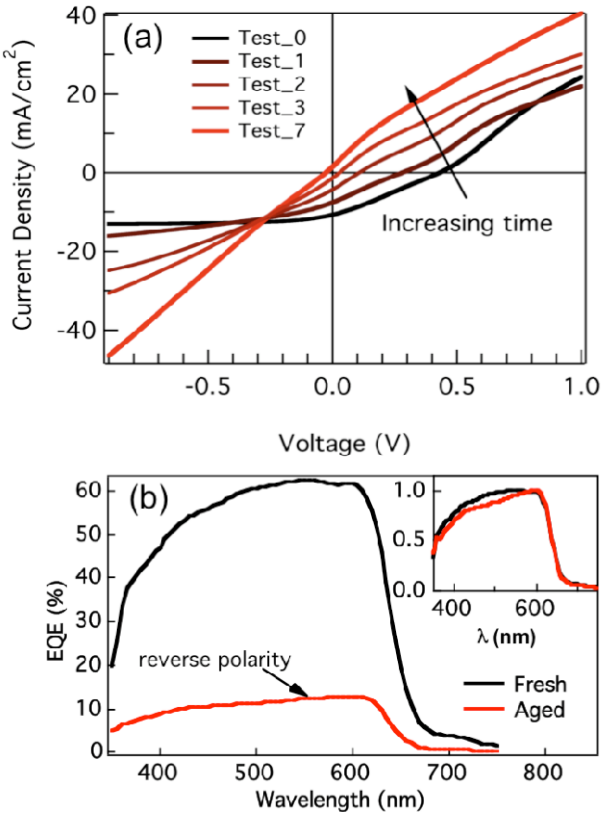

Fig. S4 (a) Change in *I-V* characteristics for an ITO/BHJ/Ag with successive testing sessions, where (black) *Test 0* was performed immediately after fabrication and (red) *Test 7* was performed 40 days after fabrication. (b) EQE for an ITO/BHJ/Ag device as (black) freshly prepared and (red) after aging, and (inset) the normalized EQE.

TOF-SIMS

Figure S5 shows TOF-SIMS depth profiles for freshly prepared and aged Ag-polymer interfaces. These samples were sputtered from the external surface of the Ag electrode proceeding into the organic layer. Fragments containing AgO, Ag_2O, AgS, and Ag_2S, are detected on the external surface of the Ag electrode, and show a peak in concentration at the Ag-polymer interface. As discussed in the manuscript, a high concentration of sulfide appears at the Ag-polymer interface even in the fresh sample, and does not show an increase upon aging. In contrast, the concentrations of oxide fragments at the Ag-polymer interface are found to increase significantly in the aged sample. This supports the notion that the work function of the aged Ag is increasing as oxide forms on the external surface as well as the buried interface. Additionally, oxygen and moisture are likely to enter the device via the electrode edges as opposed to penetrating the thickness of the Ag electrode. This is evidenced by the fact that the intensity of the oxide fragments in the bulk of the Ag is lower than either the external surface or the peak at the Ag-polymer interface.

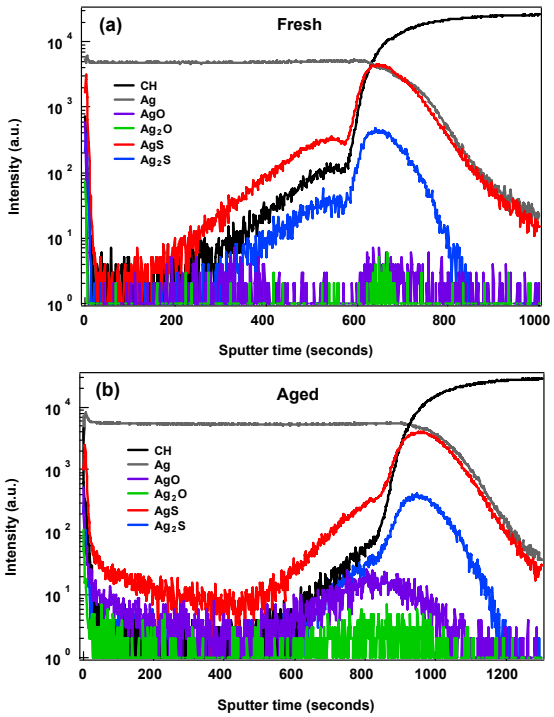

Fig. S5 TOF-SIMS depth profile for (a) freshly prepared and (b) aged Ag-polymer interface. For all Ag-containing fragments, the signal for the 109 Ag isotope is plotted. Variations in the sputter time stem from slight differences in the thickness of the thermally evaporated Ag electrodes.

EQE for Inverted ITO/ZnO/BHJ/Ag Devices

Figure S6 shows the EQE for an inverted ITO/ZnO/BHJ/Ag device. For the inverted device, both the absolute and normalized EQE plots retain their original magnitude and shape after aging.

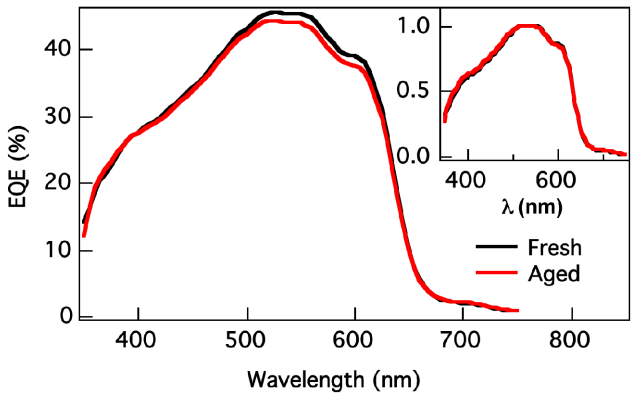

Fig. S6 EQE for an inverted device (ITO/ZnO/BHJ/Ag) as (black) freshly prepared and (red) after aging, and (inset) the normalized EQE.

Work function Change for Au vs. Ag

Figure S7 shows changes in the work function over time for films of Ag and Au deposited on P3HT coated ITO. These measurements were recorded using a Kelvin probe in air assuming a work function of 4.80 eV for Inconel metal which was used a reference. As Ag ages, the average work function increases by approximately 0.23 eV; in contrast, Au remains relatively constant. This also explains the increase in efficiency of ITO/ZnO/P3HT devices over time as shown in Fig. 5 of the manuscript.

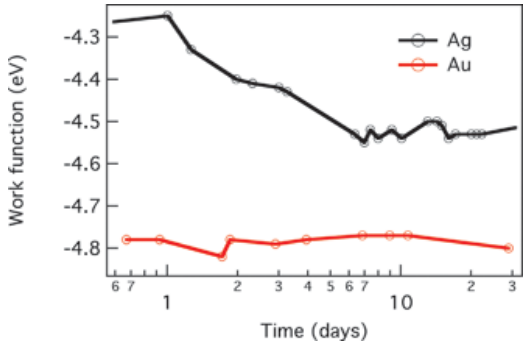

Fig. S7 Work function over time for 100 nm Ag and 50 nm Au films deposited on P3HT coated ITO substrates.